Supplementary Information for

Reactions of atmospheric particulate stabilized Criegee intermediates lead to high-molecular-weight aerosol components

MingYi Wang[†], Lei Yao[†], Jun Zheng[‡], XinKe Wang[†], JianMin Chen[†], Xin Yang[†], Douglas R. Worsnop[Δ], Neil M. Donahue[§], Lin Wang[†,*]

[†]Shanghai Key Laboratory of Atmospheric Particle Pollution and Prevention (LAP[3]), Department of Environmental Science & Engineering, Fudan University, Shanghai 200433, China

[‡]Jiangsu Key Laboratory of Atmospheric Environment Monitoring and Pollution Control, Nanjing University of Information Science & Technology, Nanjing 210044, China

[Δ]Aerodyne Research, Billerica, MA 01821, United States

[§]Center for Atmospheric Particle Studies, Carnegie Mellon University, 5000 Forbes Avenue, Pittsburgh, Pennsylvania 15213, United State

*Tel: +86-21-65643568; Fax: +86-21-65642080; E-mail: lin_wang@fudan.edu.cn

Page S1-S20

Figures S1-S11

Tables S1-S2

Contents

1. Experimental methods

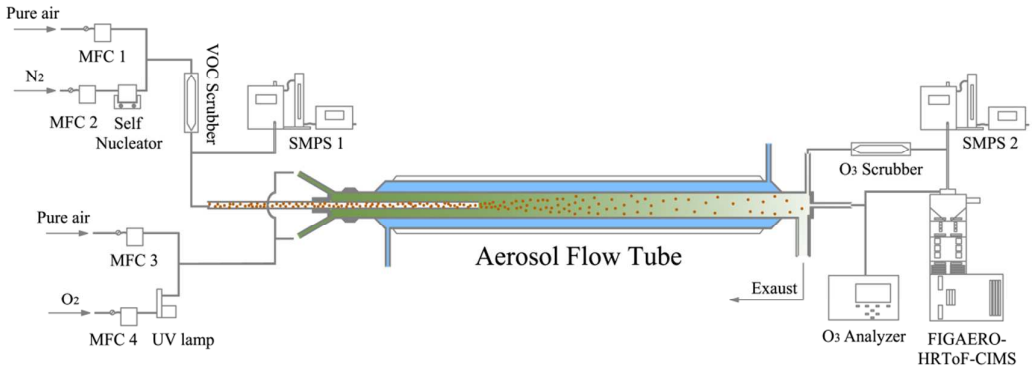

Figure S1. Schematic diagram of the aerosol flow tube apparatus.

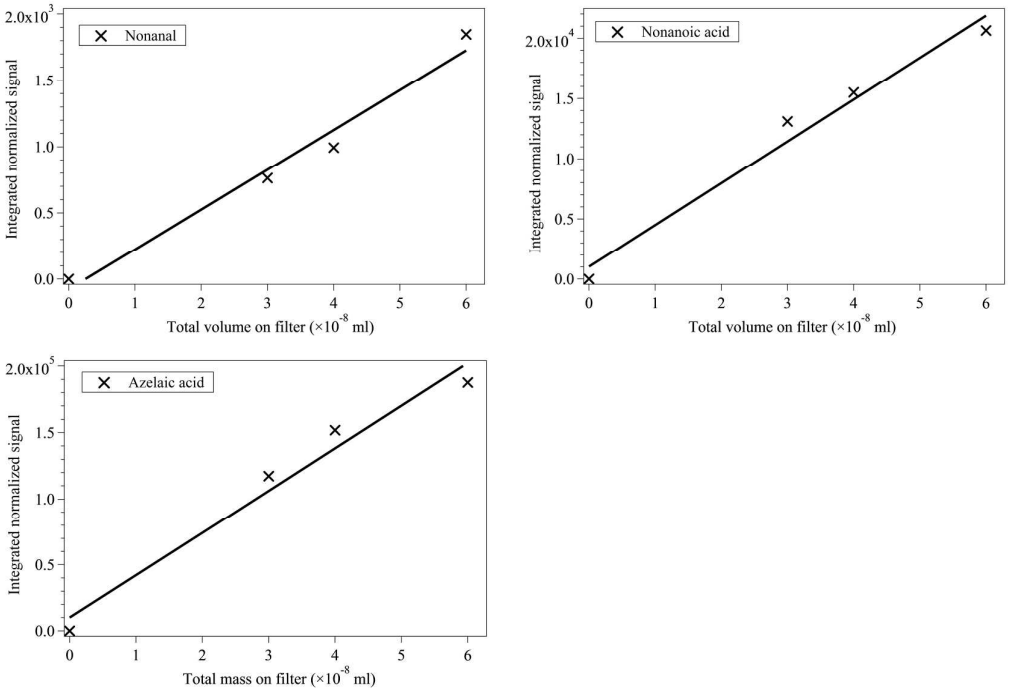

Figure S2. Calibration curves of nonanal, nonanoic and azelaic acid.

2. Kinetics

We determined the uptake coefficient γ by measuring the loss of oleic acid as a function of the ozone exposure, which is defined as the product of the contact time with the initial ozone concentration at the pseudo-first-order condition.

The oleic acid loss rate can be expressed as follows:

$$\frac{d[OL]}{dt} = -k[O_3][OL]$$

where k represents the second-order rate constant of the reaction of oleic acid with O_3 (cm^3 $molecule^{-1}$ s^{-1}), $[OL]$ and $[O_3]$ are the time dependent concentrations of the reactants (molecule cm^{-3}). In this study, the ozone concentration was ~300 ppb, which was in excess of $[OL]$ by a factor of >100, such that the ozonolysis reactions can be considered to be pseudo-first-order.

Then, integration of the above equation leads to

$$k = \frac{ln\left([OL]_0/[OL]_t\right)}{[O_3]_t \times t}$$

where $[OL]_0$ and $[OL]_t$ are the initial and final concentrations (molecule cm^{-3}) of particle-associated oleic acid, respectively, $[O_3]_t \times t$ (molecule cm^{-3} s) represents the O_3 exposure, and k is experimentally determined from the decay of oleic acid as a function of the exposure.

$[OL]_0$ can be described by

$$[OL]_0 = \frac{V_P \times \rho_{OL} \times N_A}{V \times M_{OL}}$$

where V_P/V is the particle volume density (cm^3 cm^{-3}), M_{OL} is the molar mass of oleic acid, ρ_{OL} is the density of oleic acid (0.895 g cm^{-3}), and N_A is Avogadro's constant.

The loss of oleic acid (molecule cm^{-2}) is also defined by

$$\varphi_{loss} = \frac{V}{S_P} k[O_3][OL]$$

where S_P/V is the particle surface density (cm^2 cm^{-3}).

The flux of collisions φ_{coll} (molecule s^{-1} cm^{-2}) occurring on the particle surface is defined by

$$\varphi_{coll} = \frac{[O_3] \times \omega_{O_3}}{4}$$

where ω_{O_3} is the mean speed of gas-phase O_3 (cm s^{-1}).

The uptake coefficient γ can be expressed as

$$\gamma = \frac{\varphi_{loss}}{\varphi_{coll}} = \frac{4 \times k \times D_{mean} \times \rho_{OL} \times N_A}{6 \times M_{OL} \times \omega_{O_3}}$$

where D_{mean} is the mean surface-weighted diameter of the particle distribution as measured by SMPS, and is calculated by $V_P/S_P = D_{mean}/6$ using the initial particle distribution[1].

We calculated the pseudo-first-order rate constant (k) of the ozonolysis reaction of oleic acid to be (1.19 ± 0.09) × 10^5 atm^{-1} s^{-1} for ozone exposures ranging from 0 to 1.2 × 10^{-5} atm·sec, as plotted in Figure S3. The derived uptake coefficient γ, (1.44 ± 0.11) × 10^{-3}, is reported together with values from previous studies in Table S1.

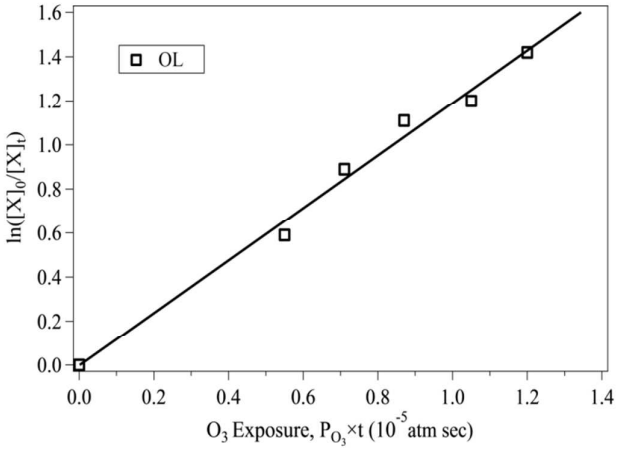

Figure S3. Reactive decay (log scale) of oleic acid (□) as a function of O_3 exposure. The solid line represents a linear fit to the data from which the rate constant *k* is determined.

Table S1. Reactive uptake coefficient and carbon-based yields (%) of the first-generation products formed from the heterogeneous ozonolysis of oleic acid.

Method	Detection	Max O_3 Exp. (atm s)	γ	Carbon-based Nominal Yield unless Other Stated								Reference
				Y_{NNgas}	$Y_{NNparticle}$	$Y_{NNtotal}$	Y_{NAgas}	$Y_{NAparticle}$	$Y_{NAtotal}$	Y_{AA}	Y_{OX}	
AFT[a]	FIGAERO-CIMS	1.2×10^{-5}	$(1.45\pm0.14)\times10^{-3}$	28.0±1.7	0[k]	28.0±1.7[k]	3.0±0.6	5.1±0.5[k]	8.1±1.1	1.9±0.1[k]	18.2±1.1[l]	This study
CFT[b]	CIMS(O_3^-)[d]	2.4×10^{-9}	$(8.3\pm0.02)\times10^{-4}$	25		27						Moise and Rudich[2]
AFT[a]	AMS[e]	1.0×10^{-4}	$(1.6\pm0.2)\times10^{-3}$									Morris *et al.*[3]
AFT[a]	SPMS[f]	1.0×10^{-3}	(0.99±0.09)-(7.3±1.5)$\times10^{-3}$									Smith *et al.*[4]
AFT[a]	Aerosol-CIMS	5.0×10^{-4}	$(7.5\pm1.2)\times10^{-4}$		42			9		6	42	Hearn and Smith[5]
CFT[b]	CIMS(O_3^-)[d]	2.1×10^{-8}	$(8.0\pm1.0)\times10^{-4}$	25								Thornberry and Abbatt[6]
AFT[a]	AMS[e]	6.6×10^{-5}						1-3		1-3	20-35	Katrib *et al.*[7]
AFT[a]	Aerosol-CIMS	5.0×10^{-4}	$(1.38\pm0.06)\times10^{-3}$									Hearn *et al.*[8]
CFT[b]	CIMS(O_3^-)[d]	1.5×10^{-8}	$(7.9\pm0.3)\times10^{-4}$									Knopf *et al.*[9]
Chamber	TDPBMS[g]	1.4×10^{-3}	$(6.1\pm5)\times10^{-4}$							4	28	Ziemann[10]
AFT[a]	AMS[e]	3.0×10^{-4}	$(1.25\pm0.2)\times10^{-3}$									Katrib *et al.*[11]
Droplets[c]	GCMS[h]&LCMS[i]	5.6×10^{-1}			30±3			7±1		6±3	14±2	Hung *et al.*[12]
AFT[a]	AMS[e]	5.0×10^{-1}						3-5		3-5	30	Shilling *et al.*[13]
AFT[a]	GCMS[h]	1.8×10^{-4}		51.7	3.3	55		2-3		3-8	7-14	Vesna *et al.*[14]
Droplets[c]	ATR-FTIR[j]	2.5×10^{-3}	$(3.2\pm1.1)\times10^{-3}$									Hung *et al.*[15]
AFT[a]	Aerosol-CIMS	3.7×10^{-5}	$(8.1\pm0.9)\times10^{-4}$									Renbaum-Wolff and Smith[16]
AFT[a]	GCMS[h]	2.0×10^{-4}	$(1.0\pm0.2)\times10^{-3}$	24.1	5.2	29.3		6.6		5.3	31.4	Mendez *et al.*[17]

[a]AFT represents aerosol flow tube; [b]CFT represents coated-wall flow tube; [c]Droplets represents droplet experiments; [d]CIMS(O_3^-) represents chemical ionization mass spectrometer for ozone detection; [e]AMS represents aerosol mass spectrometer; [f]SPMS represents single particle mass spectrometer; [g]TDPBMS represents thermal desorption particle beam mass spectrometer; [h]GCMS represents gas chromatograph mass spectrometer; [i]LCMS represents liquid chromatograph mass spectrometer; [j]ATR-FTIR represents attenuated total reflectance fourier transform

infrared spectroscopy; [k]average true yields of particle-associated nonanal, nonanoic acid, azelaic acid, respectively, based on thermal chromatogram analysis under the condition of (0.6-1.2)×10^{-5} atm·sec ozone exposure, i.e., 48.0-76.0% conversion of oleic acid; [l]the transmission efficiency of 9-oxononanoic acid (OX) during MS analysis is assumed to be identical to that of azelaic acid (TE_{AA}).

3. Single peak fitting for particulate products

Taking advantage of the high mass resolution power of the Time-of-Flight mass spectrometer and the fact that the elemental composition of these iodide-adducts is limited to carbon, hydrogen, oxygen, and iodide, we are able to assign a molecular formula to most of the major ions with a mass tolerance of < 3 ppm except for five ions < 40 ppm. Shown in Figure S4 is the single peak fitting for each of the products tentatively determined during the ozonolysis of oleic acid. Nonanoic acid is the only product that has been observed both in particles and in the gas phase.

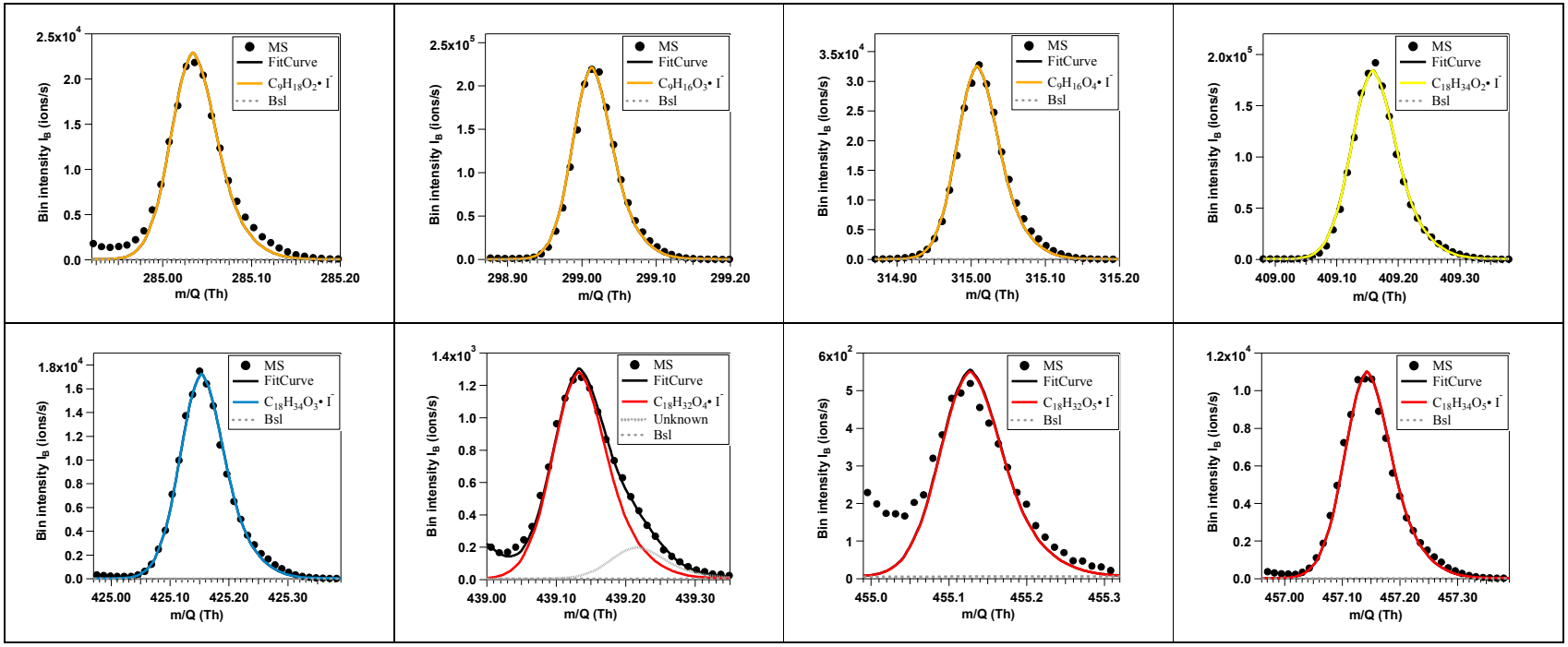

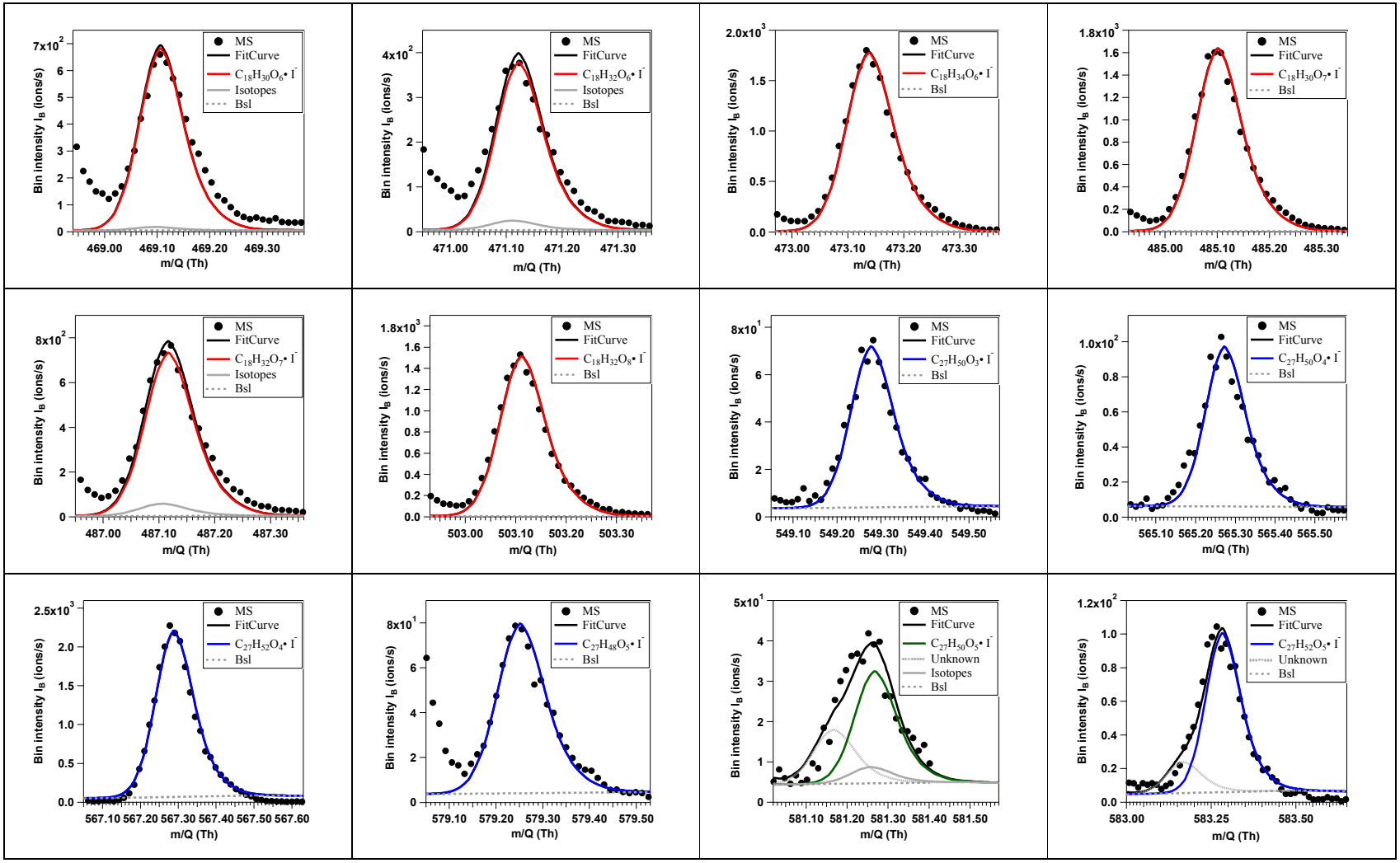
MS
FitCurve
$C_{18}H_{30}O_6 \cdot I^-$
Isotopes
Bsl
Bin intensity I_B (ions/s)
m/Q (Th)
MS
FitCurve
$C_{18}H_{32}O_6 \cdot I^-$
Isotopes
Bsl
Bin intensity I_B (ions/s)
m/Q (Th)
MS
FitCurve
$C_{18}H_{34}O_6 \cdot I^-$
Bsl
Bin intensity I_B (ions/s)
m/Q (Th)
MS
FitCurve
$C_{18}H_{30}O_7 \cdot I^-$
Bsl
Bin intensity I_B (ions/s)
m/Q (Th)
MS
FitCurve
$C_{18}H_{32}O_7 \cdot I^-$
Isotopes
Bsl
Bin intensity I_B (ions/s)
m/Q (Th)
MS
FitCurve
$C_{18}H_{32}O_8 \cdot I^-$
Bsl
Bin intensity I_B (ions/s)
m/Q (Th)
MS
FitCurve
$C_{27}H_{50}O_5 \cdot I^-$
Bsl
Bin intensity I_B (ions/s)
m/Q (Th)
MS
FitCurve
$C_{27}H_{50}O_4 \cdot I^-$
Bsl
Bin intensity I_B (ions/s)
m/Q (Th)
MS
FitCurve
$C_{27}H_{52}O_4 \cdot I^-$
Bsl
Bin intensity I_B (ions/s)
m/Q (Th)
MS
FitCurve
$C_{27}H_{48}O_5 \cdot I^-$
Bsl
Bin intensity I_B (ions/s)
m/Q (Th)
MS
FitCurve
$C_{27}H_{50}O_5 \cdot I^-$
Unknown
Isotopes
Bsl
Bin intensity I_B (ions/s)
m/Q (Th)
MS
FitCurve
$C_{27}H_{52}O_5 \cdot I^-$
Unknown
Bsl
Bin intensity I_B (ions/s)
m/Q (Th)

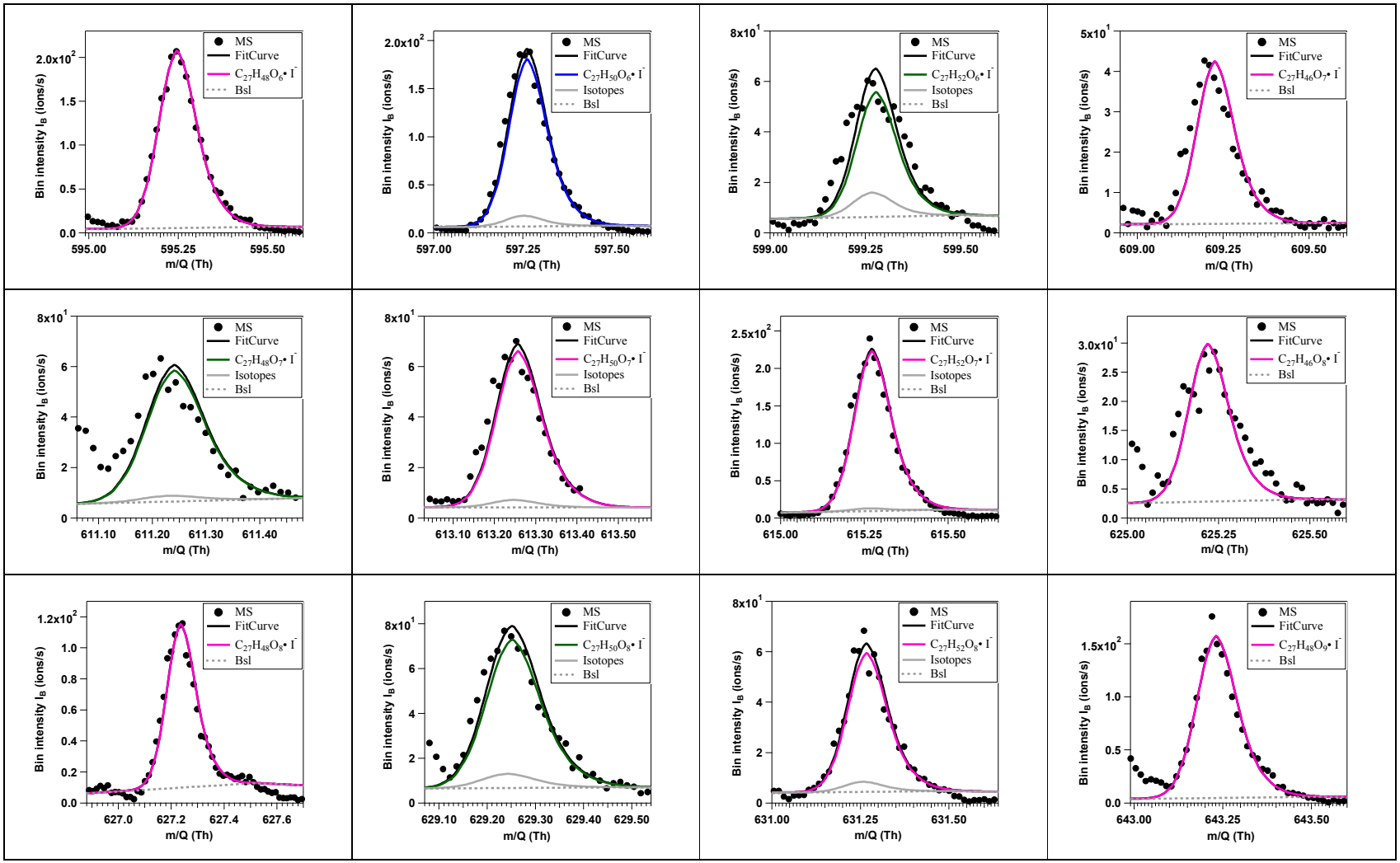
MS
FitCurve
$C_{27}H_{48}O_6 \bullet I^-$
Bsl
Bin intensity I_B (ions/s)
m/Q (Th)
MS
FitCurve
$C_{27}H_{50}O_6 \bullet I^-$
Isotopes
Bsl
Bin intensity I_B (ions/s)
m/Q (Th)
MS
FitCurve
$C_{27}H_{52}O_6 \bullet I^-$
Isotopes
Bsl
Bin intensity I_B (ions/s)
m/Q (Th)
MS
FitCurve
$C_{27}H_{46}O_7 \bullet I^-$
Bsl
Bin intensity I_B (ions/s)
m/Q (Th)
MS
FitCurve
$C_{27}H_{48}O_7 \bullet I^-$
Isotopes
Bsl
Bin intensity I_B (ions/s)
m/Q (Th)
MS
FitCurve
$C_{27}H_{50}O_7 \bullet I^-$
Isotopes
Bsl
Bin intensity I_B (ions/s)
m/Q (Th)
MS
FitCurve
$C_{27}H_{52}O_7 \bullet I^-$
Isotopes
Bsl
Bin intensity I_B (ions/s)
m/Q (Th)
MS
FitCurve
$C_{27}H_{46}O_8 \bullet I^-$
Bsl
Bin intensity I_B (ions/s)
m/Q (Th)
MS
FitCurve
$C_{27}H_{48}O_8 \bullet I^-$
Bsl
Bin intensity I_B (ions/s)
m/Q (Th)
MS
FitCurve
$C_{27}H_{50}O_8 \bullet I^-$
Isotopes
Bsl
Bin intensity I_B (ions/s)
m/Q (Th)
MS
FitCurve
$C_{27}H_{52}O_8 \bullet I^-$
Isotopes
Bsl
Bin intensity I_B (ions/s)
m/Q (Th)
MS
FitCurve
$C_{27}H_{48}O_9 \bullet I^-$
Bsl
Bin intensity I_B (ions/s)
m/Q (Th)

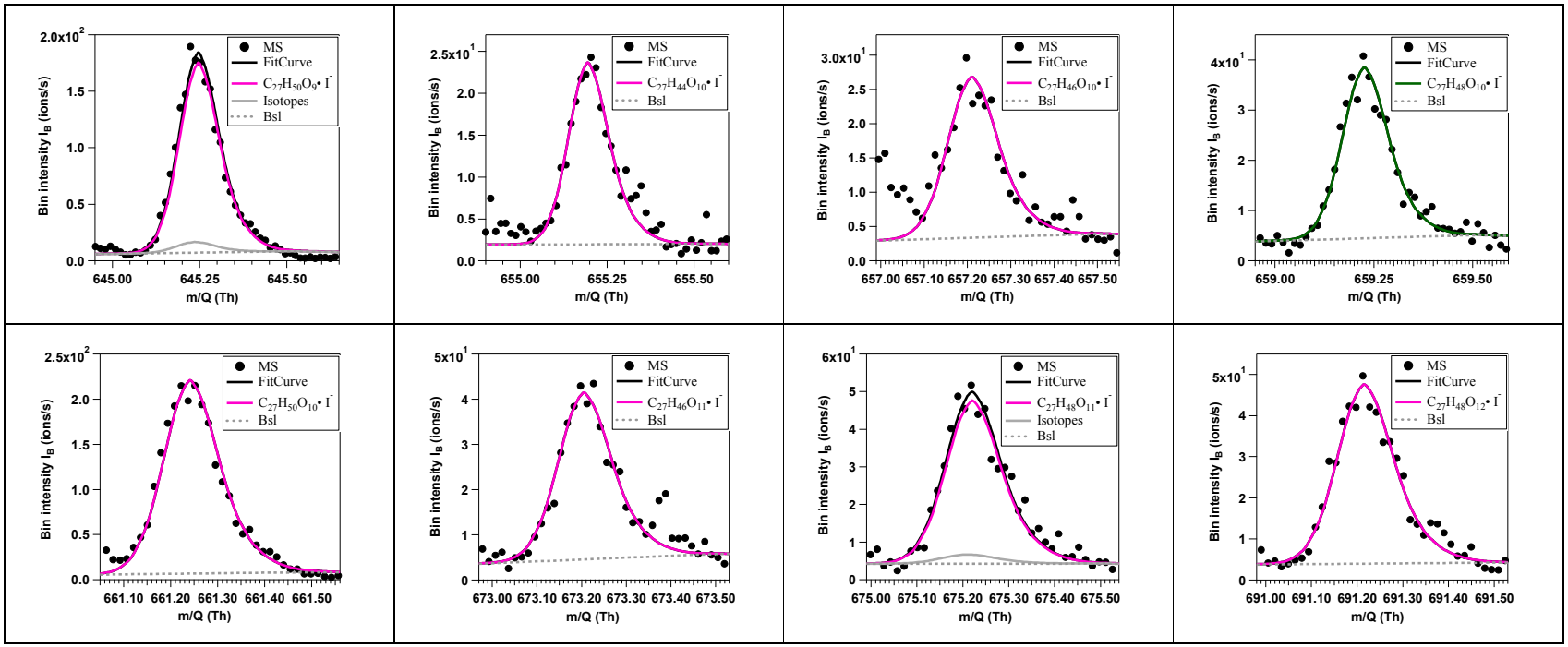

Figure S4. Single peak fitting for each of the tentatively determined products from ozonolysis of oleic acid

4. Reaction mechanism for ozonolysis of oleic acid

We propose a stabilized Criegee intermediate (SCI)-based reaction mechanism to elucidate the formation routes of all observed products. In the main text, Figure 2 is a flowchart from the parent oleic acid to the first-, second- and multi-generation products with one molecular structure as an example for each category. Here, we present detailed formation routes for all observed products. Figure S5A illustrates that the first-generation carbonyls (nonanal or 9-oxononanoic acid) and acids (nonanoic acid or azelaic acid or 9-oxononanoic acid) react with SCIs to form secondary ozonides (SOZ) and α-acyloxyalkyl hydroperoxides (AAHP), which further react with another SCI to form SOZ-AAHP and AAHP-AAHP, respectively, and that the self-reaction of SCIs leads to diperoxides (DP) and then DP-AAHP.

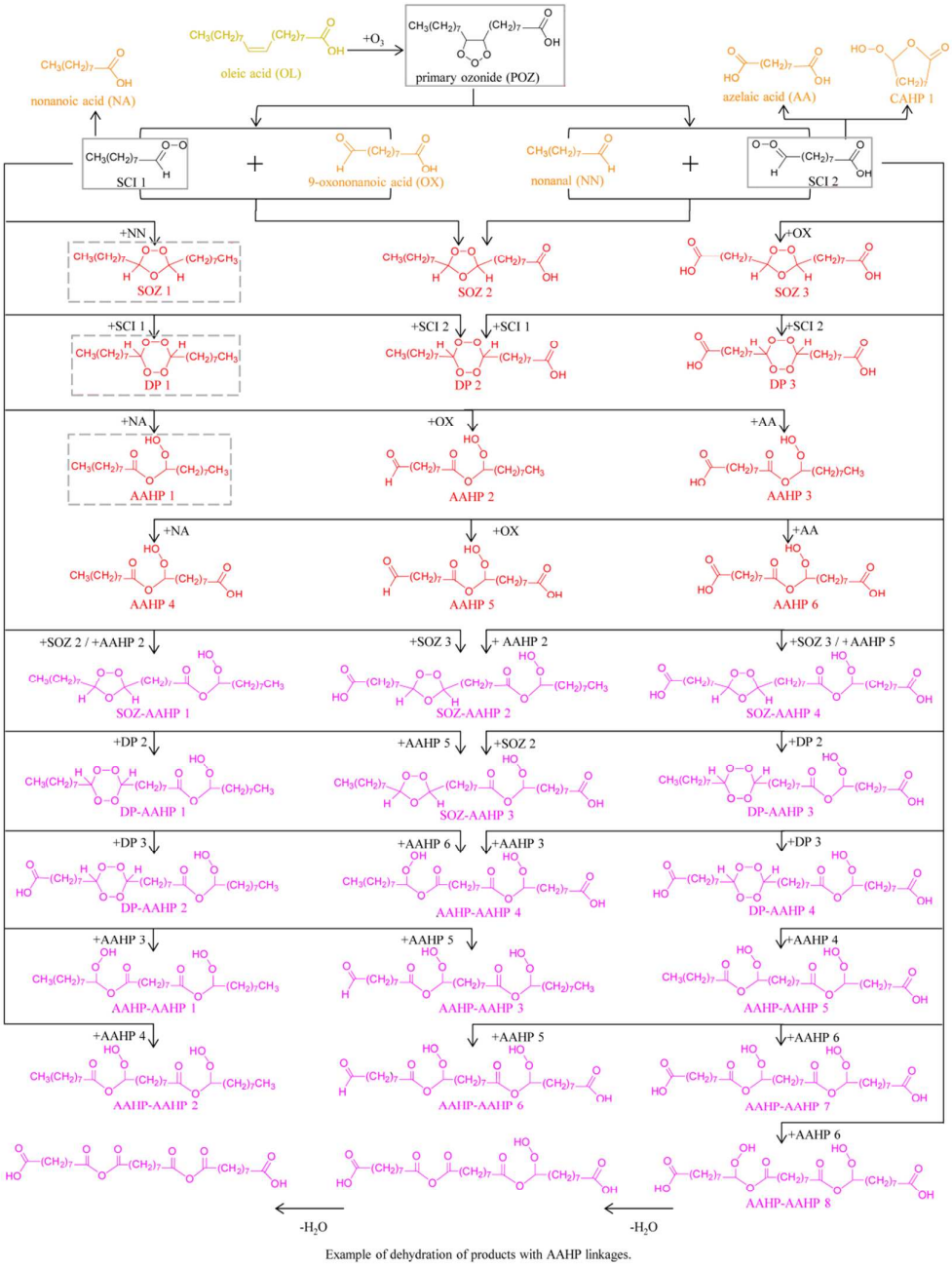

Figure S5A. Reaction pathways between SCIs and the first-generation products.

Figure S5B shows that SCIs react with an intact oleic acid to form an OL-AAHP or a dioxolane (DO), depending on whether the SCIs react with the carboxylic acid group or the double bond, and that SCIs react with OL-AAHPs and DO, respectively, to form OL-AAHP-AAHP and DO-AAHP. In addition, the dioxolane ring in DO is subject to decomposition, giving rise to oxooctadecanoic acid (OO), and OO reacts with SCIs stepwise to form OO-AAHP and OO-AAHP-AAHP.

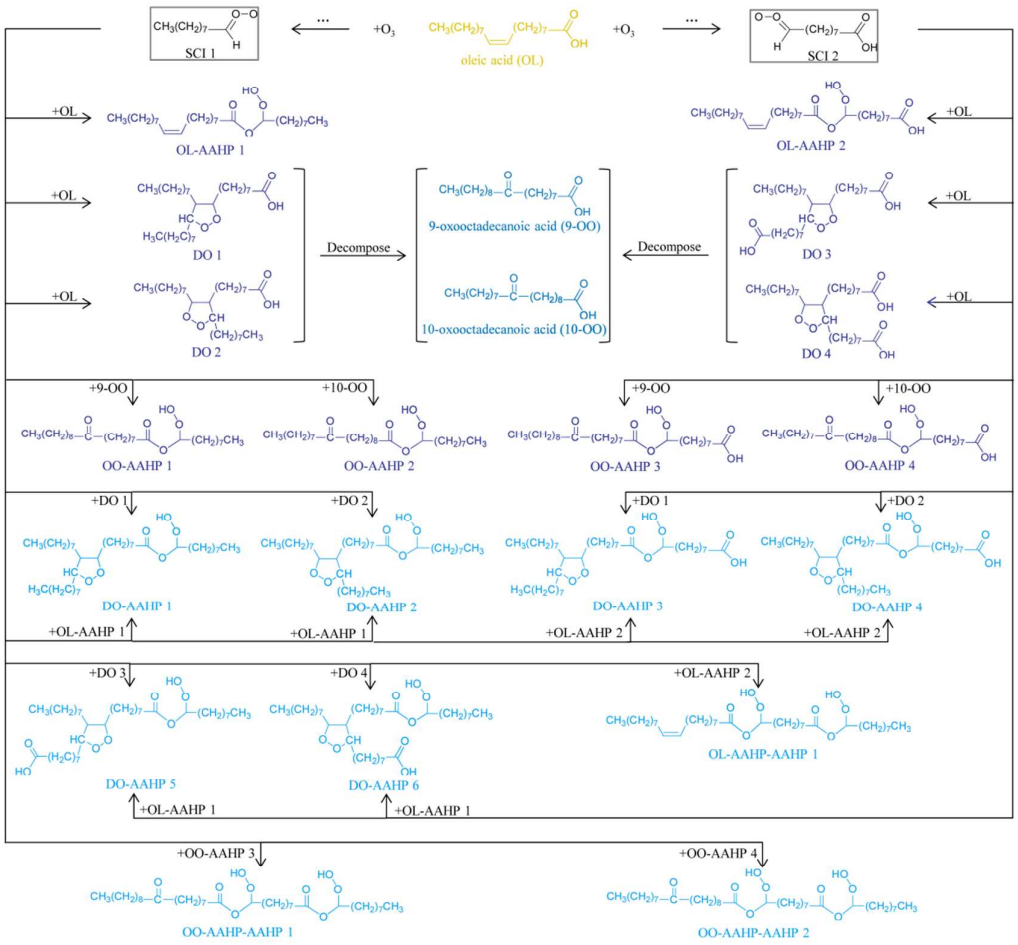

Figure S5B. Reaction pathways between SCIs and an intact oleic acid.

Figure S5C shows that AAHPs react with a first-generation carbonyl (nonanal or 9-oxononanoic acid) to form peroxyhemiacetals (PHAs), and that PHAs react with a first-generation carboxylic acid (nonanoic acid or azelaic acid or 9-oxononanoic acid) to form bis(α-acyloxy-α-alkyl)peroxides (BAAPs).

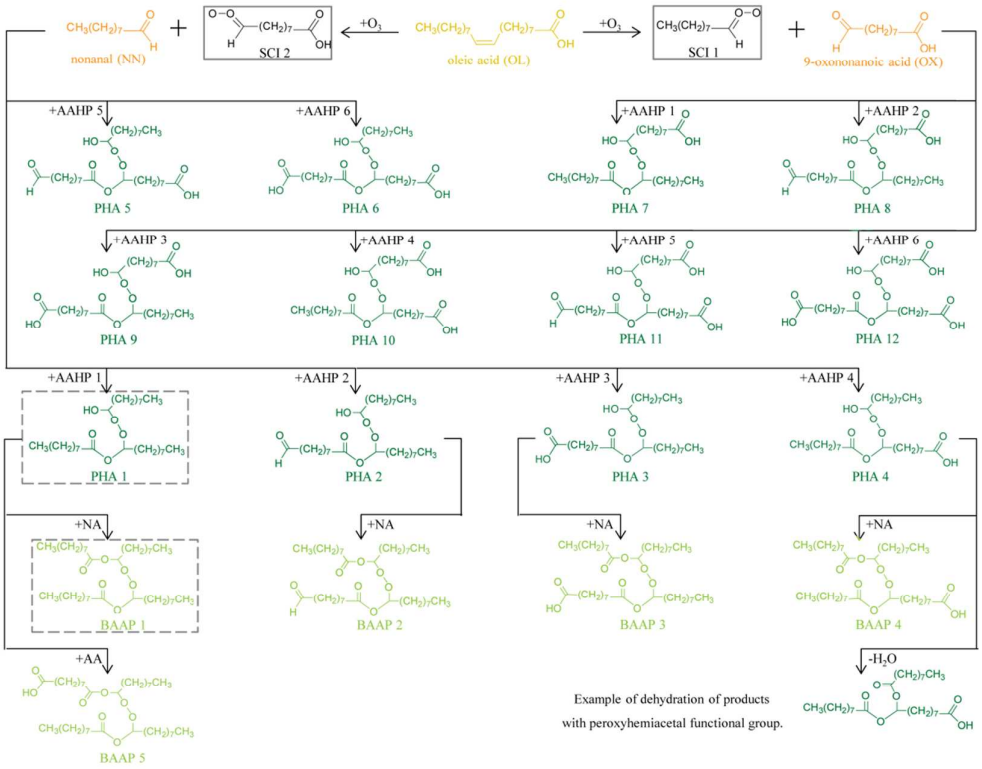

Figure S5C. Reaction pathways for PHAs and BAAPs

5. Ozonolysis of Erucic acid

We studied the ozonolysis of erucic acid (EA), a C_{22} ω-13 unsaturated carboxylic acid to test the proposed reaction mechanism for ozonolysis of oleic acid because of the similarity in molecular structure between the two fatty acids. We identified an analogous series of products, except for those whose mass-charge-ratios exceed 800 amu (i.e. whose molecular weight exceed 670 Da.) where the signal-noise-ratio does not allow identification of a product. In Figure S6, we present the mass spectra of reacted EA particles in the same color-coding we use for oleic acid.

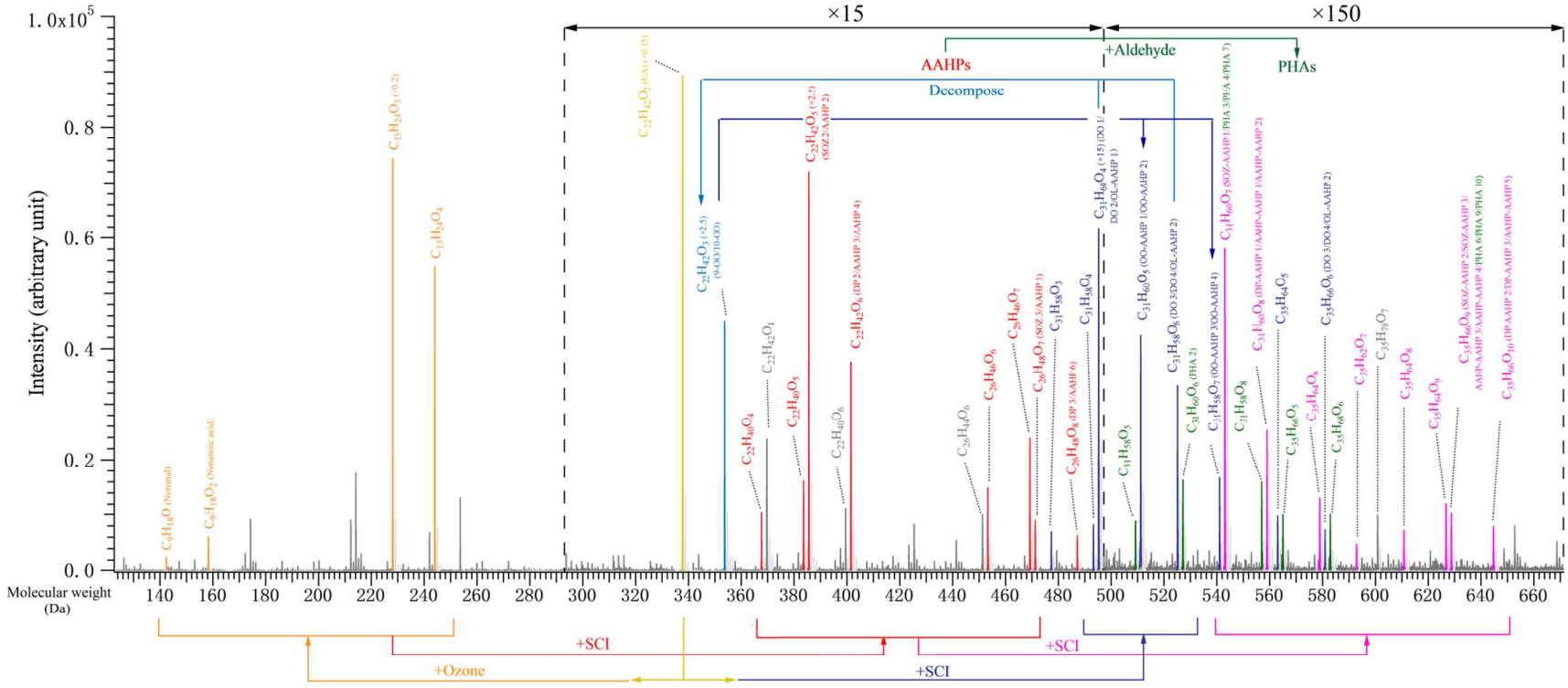

Figure S6. A typical blank-corrected mass spectrum for ozonolysis of erucic acid.

6. Ozonolysis of two-component mixture particles

To further test the proposed reaction mechanism for ozonolysis of oleic acid, we generated a series of two-component mixture particles, exposed them to ozone, and subsequently analyzed them by FIGAERO-HRToF-CIMS. For ozonolysis of 37.5% oleic acid / 62.5% 1-dodecanol mixtures (mol/mol), we did not observe products other than those from ozonolysis of oleic acid. Ozonolysis of 37.5% oleic acid / 62.5% 1-octadecene (mol/mol) leads to a $C_{18}H_{36}O$ (1-octadecanal or 2-octadecanone, Figure S7), presumably formed from the decomposition of a DO analogue that is derived from the addition of an oleic acid-derived SCI to the double bond of 1-octadecene. Also, Ozonolysis of 1-octadecene forms particulate products including $C_{17}H_{34}O_2$ (1-heptadecanoic acid), $C_{18}H_{36}O_3$ (potentially a SOZ), $C_{26}H_{50}O_5$ (potentially a SOZ or DP or AAHP), and $C_{26}H_{50}O_6$ (potentially a DP or AAHP).

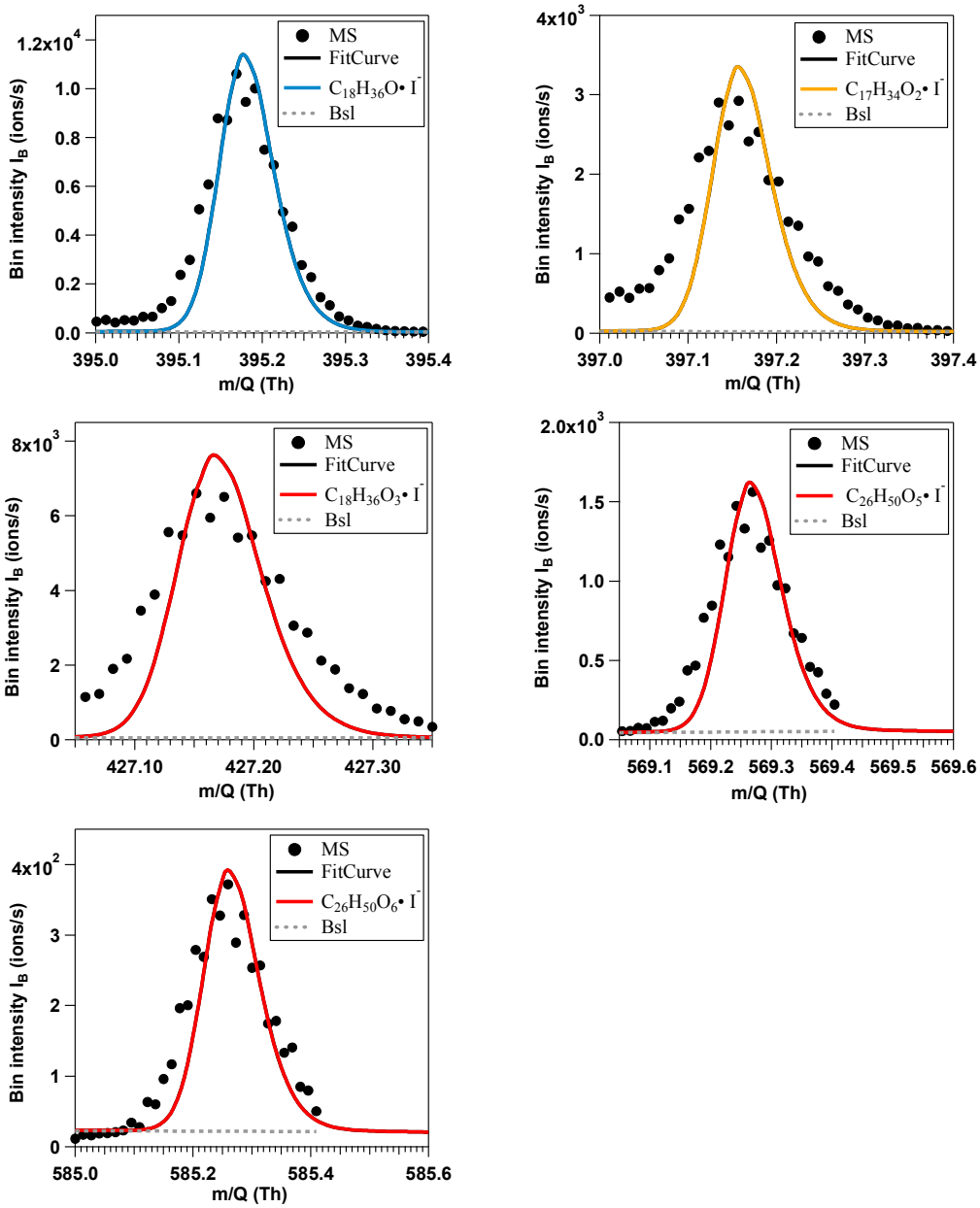

Figure S7. Single peak fitting for new products identified during ozonolysis of oleic acid/1-octadecene particles.

When we exposed 37.5% oleic acid / 62.5% 1-dodecyl aldehyde (mol/mol) particles to ozone, we observed $C_{21}H_{42}O_3$ and $C_{21}H_{40}O_5$, potentially new SOZ species formed from reactions of oleic-acid derived SCIs and 1-dodecyl aldehyde (Figure S8) confirming the SCI + aldehyde pathway.

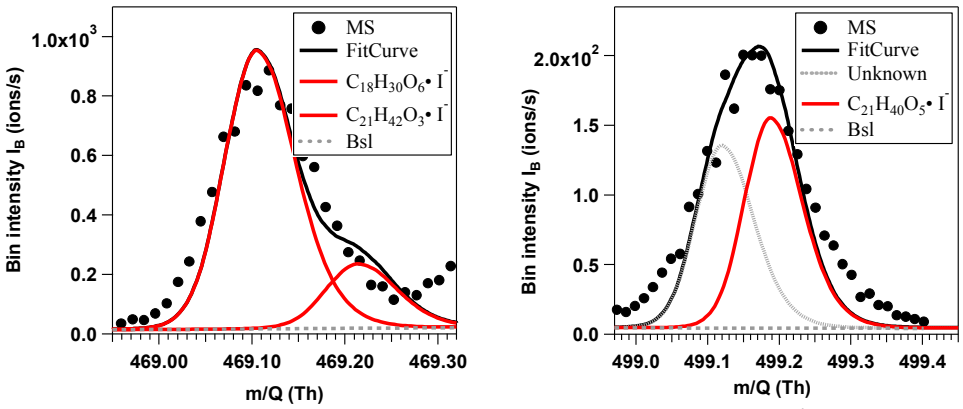

Figure S8. Single peak fitting for new products identified during ozonolysis of oleic-acid/1-dodecyl aldehyde particles.

In the case of 37.5% oleic acid / 62.5% 2-hexyldecanoic acid (mol/mol), the presence of $C_{25}H_{50}O_4$ and $C_{25}H_{48}O_6$, presumably new AAHP species formed from oleic acid-derived SCIs and 2-hexyldecanoic acid, is evident in Figure S9, validating the SCIs + acid pathway. Also, $C_{25}H_{48}O_3$ and $C_{25}H_{46}O_5$, the dehydration products from $C_{25}H_{50}O_4$ and $C_{25}H_{48}O_6$, respectively, are observed.

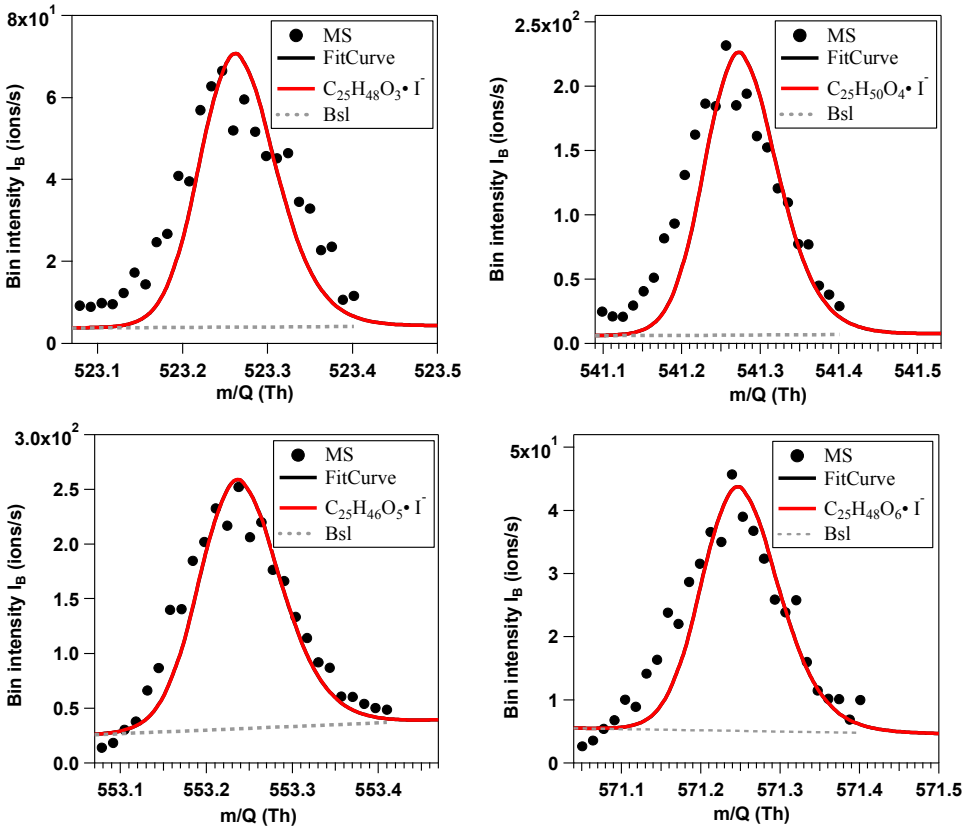

Figure S9. Single peak fitting of new products identified during ozonolysis of oleic acid/2-hexyldecanoic acid particles.

7. True yields of the C_9 products

With the understanding that thermal decomposition of higher generation particulate products contributes to the measured total abundance of C_9 products (nonanal, NN; nonanoic acid, NA; azelaic acid, AA; and 9-oxononanoic acid, OX) during the FIGAERO analysis, we conclude that the true yields of particulate C_9 products can be obtained by subtracting the overestimated part (the latter signals for the double peaks) from the total. We present time-resolved true carbon yields of the particulate C_9 products after such corrections in Figure S10, together with yields of gaseous C_9 products. It should be noted that we do not report $Y_{NNparticle}$ because all observed particulate nonanol comes from the thermal decomposition of higher generation products.

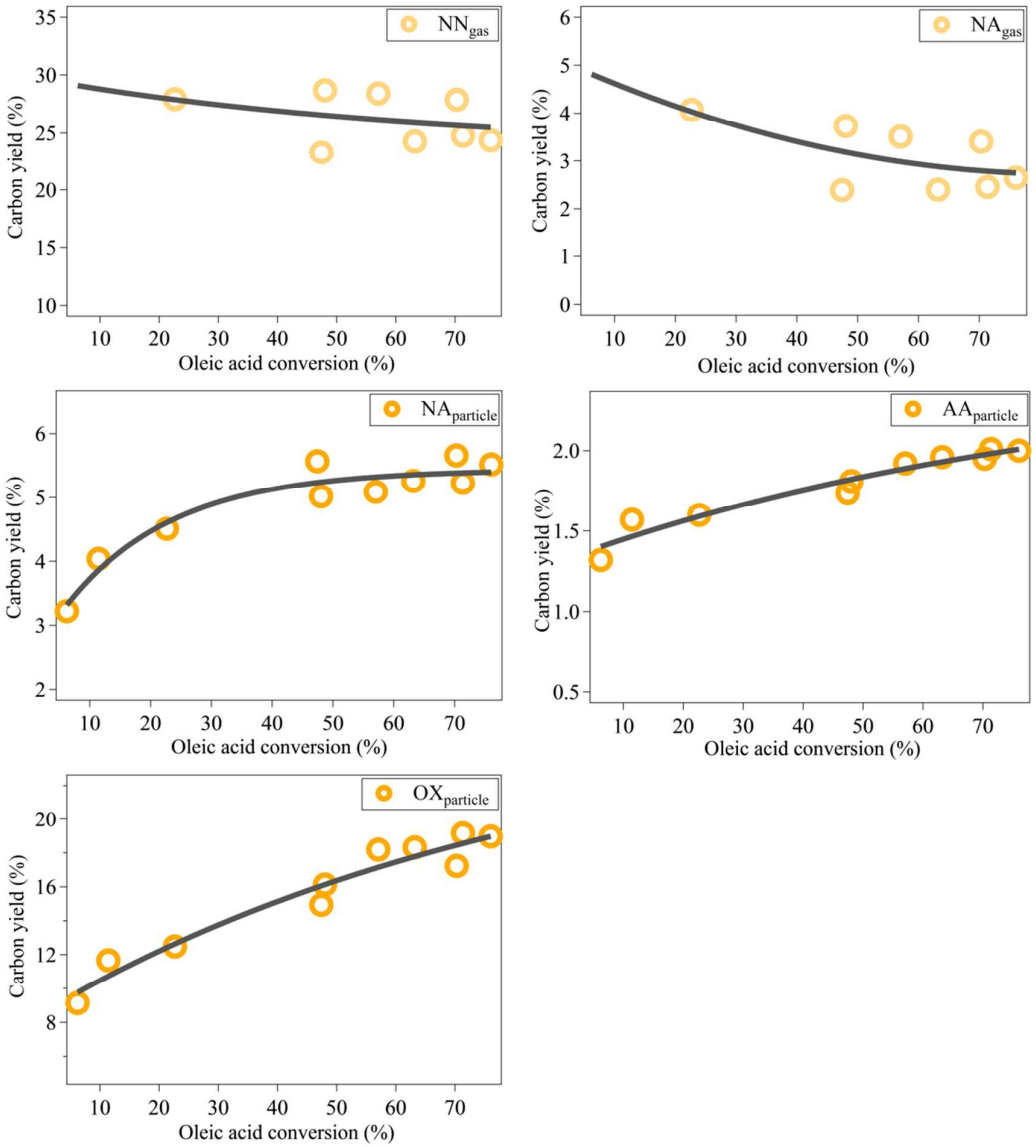

Figure S10. Time-resolved true yields of the C_9 products. The transmission efficiency of 9-oxononanoic acid during MS analysis is assumed to be identical to that of azelaic acid (TE_{AA}). Lines are plotted to guide the eye.

8. Branching ratio

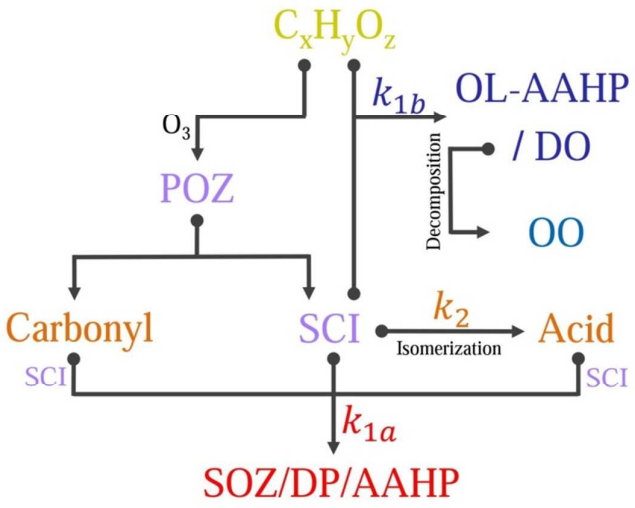

Figure S11. Simplified mechanisms for reactions of SCIs with the C_9 species and oleic acid, and isomerization of SCIs.

We are not able to determine the exact sensitivity for each compound without authentic standards. A recent quantum chemical study reported that a strongly bound iodide-molecule cluster is more likely to be detected at maximum sensitivity by CIMS[18]. Since these C_{18} products in our model calculation mostly contain multiple hydroperoxide functional groups, their detection likely reaches the same maximum transmission efficiency. We hereby make an assumption in our manuscript that the transmission efficiencies of 9-oxononanoic acid (TE_{OX}), OO, SOZ, DP, and AAHP (TE_{C18}) are the same as that of azelaic acid (TE_{AA}).

We perform a sensitivity analysis to test the sensitivity of the regression results to the variables. While $TE_{OX}/TE_{AA} = 1$ leads to a consistent yield of 9-oxononanoic acid with previous studies[7, 10, 12-14, 17], TE_{C18}/TE_{AA}, the transmission efficiency ratio of the C_{18} products ($[OO]$, $[SOZ]$, $[DP]$ and $[AAHP]$) to azelaic acid ($[AA]$) in our time of flight mass spectrometer is set in range of 1/3 to 3, and f is from 0 to 50%, respectively. This analysis gives variable but similar k_{1a}/k_2 and k_{1b}/k_2 values as shown in Table S2A-B, indicating that the general trend of the time-resolved yields of later-generation products will be preserved.

Table S2A. Values of k_{1a}/k_2 under various scenarios of f and TE_{C18}

k_{1a}/k_2	$TE_{C18} = 1/3 \times TE_{AA}$	$TE_{C18} = TE_{AA}$	$TE_{C18} = 3 \times TE_{AA}$
$f = 0$	0.26±0.24	0.42±0.08	0.48±0.02
$f = 30\%$	0.07±0.15	0.18±0.05	0.21±0.02
$f = 50\%$	0.008±0.12	0.09±0.04	0.12±0.01

Table S2B. Values of k_{1b}/k_2 under various scenarios of f and TE_{C18}

k_{1b}/k_2	$TE_{C18} = 1/3 \times TE_{AA}$	$TE_{C18} = TE_{AA}$	$TE_{C18} = 3 \times TE_{AA}$
$f = 0$	3.18±0.23	1.45±0.08	0.88±0.02
$f = 30\%$	1.96±0.15	0.83±0.05	0.46±0.02
$f = 50\%$	1.52±0.12	0.61±0.04	0.31±0.01

REFERENCES

1. Smith, J. D.; Kroll, J. H.; Cappa, C. D.; Che, D. L.; Liu, C. L.; Ahmed, M.; Leone, S. R.; Worsnop, D. R.; Wilson, K. R., The heterogeneous reaction of hydroxyl radicals with sub-micron squalane particles: A model system for understanding the oxidative aging of ambient aerosols. *Atmos. Chem. Phys.* **2009,** *9*, (9), 3209-3222.
2. Moise, T.; Rudich, Y., Reactive uptake of ozone by aerosol-associated unsaturated fatty acids: Kinetics, mechanism, and products. *J. Phys. Chem. A* **2002,** *106*, (27), 6469-6476.
3. Morris, J. W.; Davidovits, P.; Jayne, J. T.; Jimenez, J. L.; Shi, Q.; Kolb, C. E.; Worsnop, D. R.; Barney, W. S.; Cass, G., Kinetics of submicron oleic acid aerosols with ozone: A novel aerosol mass spectrometric technique. *Geophys. Res. Lett.* **2002,** *29*, (9) *, 1357, doi:10.1029/2002GL014692*.
4. Smith, G. D.; Woods, E.; DeForest, C. L.; Baer, T.; Miller, R. E., Reactive uptake of ozone by oleic acid aerosol particles: Application of single-particle mass spectrometry to heterogeneous reaction kinetics. *J. Phys. Chem. A* **2002,** *106*, (35), 8085-8095.
5. Hearn, J. D.; Smith, G. D., Kinetics and product studies for ozonolysis reactions of organic particles using aerosol CIMS. *J. Phys. Chem. A* **2004,** *108*, (45), 10019-10029.
6. Thornberry, T.; Abbatt, J. P. D., Heterogeneous reaction of ozone with liquid unsaturated fatty acids: Detailed kinetics and gas-phase product studies. *Phys. Chem. Chem. Phys.* **2004,** *6*, (1), 84-93.
7. Katrib, Y.; Martin, S. T.; Hung, H. M.; Rudich, Y.; Zhang, H. Z.; Slowik, J. G.; Davidovits, P.; Jayne, J. T.; Worsnop, D. R., Products and mechanisms of ozone reactions with oleic acid for aerosol particles having core-shell morphologies. *J. Phys. Chem. A* **2004,** *108*, (32), 6686-6695.
8. Hearn, J. D.; Lovett, A. J.; Smith, G. D., Ozonolysis of oleic acid particles: Evidence for a surface reaction and secondary reactions involving Criegee intermediates. *Phys. Chem. Chem. Phys.* **2005,** *7*, (3), 501-511.
9. Knopf, D. A.; Anthony, L. M.; Bertram, A. K., Reactive uptake of O_3 by multicomponent and multiphase mixtures containing oleic acid. *J. Phys. Chem. A* **2005,** *109*, (25), 5579-5589.
10. Ziemann, P. J., Aerosol products, mechanisms, and kinetics of heterogeneous reactions of ozone with oleic acid in pure and mixed particles. *Faraday Discuss.* **2005,** *130*, 469.
11. Katrib, Y.; Biskos, G.; Buseck, P. R.; Davidovits, P.; Jayne, J. T.; Mochida, M.; Wise, M. E.; Worsnop, D. R.; Martin, S. T., Ozonolysis of mixed oleic-acid/stearic-acid particles: Reaction kinetics and chemical morphology. *J. Phys. Chem. A* **2005,** *109*, (48), 10910-10919.
12. Hung, H. M.; Katrib, Y.; Martin, S. T., Products and mechanisms of the reaction of oleic acid with ozone and nitrate radical. *J. Phys. Chem. A* **2005,** *109*, (20), 4517-4530.
13. Shilling, J. E.; King, S. M.; Mochida, M.; Martin, S. T., Mass spectral evidence that small changes in composition caused by oxidative aging processes alter aerosol CCN properties. *J. Phys. Chem. A* **2007,** *111*, (17), 3358-3368.
14. Vesna, O.; Sax, M.; Kalberer, M.; Gaschen, A.; Ammann, M., Product study of oleic acid ozonolysis as function of humidity. *Atmos. Environ.* **2009,** *43*, (24), 3662-3669.
15. Hung, H. M.; Tang, C. W., Effects of temperature and physical state on heterogeneous oxidation of oleic acid droplets with ozone. *J. Phys. Chem. A* **2010,** *114*, (50), 13104-13112.
16. Renbaum-Wolff, L.; Smith, G. D., "Virtual injector" flow tube method for measuring relative rates kinetics of gas-phase and aerosol species. *J. Phys. Chem. A* **2012,** *116*, (25), 6664-74.
17. Mendez, M.; Visez, N.; Gosselin, S.; Crenn, V.; Riffault, V.; Petitprez, D., Reactive and nonreactive ozone uptake during aging of oleic acid particles. *J. Phys. Chem. A* **2014,** *118*, (40), 9471-81.
18. Iyer, S.; Lopez-Hilfiker, F.; Lee, B. H.; Thornton, J. A.; Kurten, T., Modeling the detection of organic and inorganic compounds using iodide-based chemical ionization. *J. Phys. Chem. A* **2016,** *120*, (4), 576-587.